Perturbation Estimation Based Nonlinear Adaptive Control of VSC Flexible Excitation System

Ning Yang, Qi Zeng, Xin Yin, Weiyu Wang, Pingliang Zeng, Lin Jiang

***Abstract*—A new type of flexible excitation system (FES) is proposed by using fully-controlled power electronic devices such as IGBTs to replace the half controlled devices in the conventional static excitation system, which has the merit of independent control of rotor angle and terminal voltage of the synchronous generator (SG). This paper proposes nonlinear adaptive control (NAC) strategies for SG with FES in a single machine infinite bus (SMIB) system. External disturbances and the uncertainties of all parameters as well as modelling are defined as lumped perturbation terms and estimated by perturbation observers (POs) or state and perturbation observer (SPO). The estimated perturbation terms are used to compensate the real perturbations and achieve a model-independent and robust NAC. Merits of the FES against the conventional static excitation system and effectiveness of the proposed NAC scheme against the accurate model based multi-variable feedback linearization control (MFLC) are verified via small-signal stability analysis and simulation studies. The simulation results have shown that the proposed NAC can achieve superior control performance with less states feedback during a three-phase short circuit and better robustness against parameter uncertainties, compared with linear control and MFLC.**

NOMENCLATURE

δ	Rotor angle of synchronous generator
ω	Rotor speed of synchronous generator
ω_0	Nominal synchronous speed
b_{VSC}	The equivalent compensated admittance
b^*_{VSC}	The reference of equivalent compensated admittance
D	Damping
E_{fd}	Synchronous generator field voltage
E_q	Internal voltage in q-axis of synchronous generator
E'_q	Internal transient voltage in q-axis of synchronous generator
P_m	Input mechanical power of synchronous generator
P_t	Electrical power of synchronous generator
T'_{do}	d-axis OC transient time constant
T_j	Rotor inertia constant
T_Q	The inherent time constant of FES
U_b	Infinite bus voltage
U_t	Terminal voltage of synchronous generator
v_{td}, v_{tq}	Stator voltages in d- and q-axis of synchronous generator, respectively
x_d	d-axis synchronous reactance
x'_d	d-axis transient reactance
x_L	Line reactance
x_q	q-axis synchronous reactance
x_t	reactance of the transformer

This paper is partially funded by EPSRC project (EP/J014249/1) and 2018 Huzhou South Taihu Elite Program Leading Innovation Team Project. N.Yang, Q. Zeng, X. Yin and L. Jiang are with the Department of Electrical Engineering and Electronics, University of Liverpool, Liverpool, L69 3GJ, UK (E-mail: Ning.Yang@liverpool.ac.uk, psqzeng2@liverpool.ac.uk, leoxinyin@hotmail.com, ljiang@liv.ac.uk.)

W. Wang is with the School of Electrical and Information Engineering, Changsha University of Science and Technology, Changsha, 410114, China (e-mail: wywang@csust.edu.cn).

P. Zeng is with the School of Automation, Hangzhou Dianzi University, Hangzhou, 310018, China (E-mail: plzeng@hotmail.com).

I. INTRODUCTION

Static excitation systems using half-controlled thyristor based rectifiers have been widely installed on synchronous generators (SGs) in the convectional power system as one of the most effective and economic measures for stability and voltage support [1], [2]. Moreover, although more SGs will be replaced by non-dispatchable and non-synchronous renewable generations in the future power system, traditional synchronous generation will remain a relatively high share in many power grids. Thus the excitation system of SG will still contribute as a key role to support the grid stability [6], [7]. However, besides the numerous benefits, SGs with static excitation system encounters some problems, such as power quality problem like line voltage notching and line current distorting due to the usage of the half-controlled thyristors [3], [4]; and compromised regulation performance of two control objectives of the terminal voltage and the rotor angle due to using only the field excitation voltage as the control variable [5].

With the development of power electronics, a flexible excitation system (FES) has been proposed for SG by using fully-controlled power electronic devices such as IGBT to replace thyristors used in conventional excitation systems [8]. As shown in Fig. 1, the FES consists of a front-end voltage source converter (VSC), a back-end DC/DC chopper, and a step-down transformer [9]. It can provide independent control of the excitation voltage from the chopper and the reactive power control from the VSC, which enable independent control of rotor angle and terminal voltage of SG; while the conventional static excitation system can only use the excitation voltage to control both the rotor angle and the terminal voltage [10]. Moreover, the fully controlled VSC can achieve better power quality by regulating the input current sinusoidally and reducing harmonic distortion [11], [12].

Many control methods have been proposed to ensure the satisfactory dynamic performance of SG with FES, such as vector control [9], linear optimal control [13], and lead-lag phase compensation based control[14], [15]. The mechanism of the FES to enhance power system stability is demonstrated in [9], in which FES is controlled by vector control with PI loops and verified by simulation studies. FES with linear

optimal controller and experimental verification are given in [13], which show that transient performance and steady-state stability limit can be improved from the FES, compared with the conventional excitation systems. Phase compensation based design is applied to two independent design of a PSS and a reactive power control of the FES [14]. Then, to reduce the coupling effects between those two control loops, a coordinated optimisation method is proposed to tune gains of those two loops, and implemented and tested at a 55-MW hydropower generator [15]. As linear control strategies are derived and optimised based on one operating point, their performance will be degraded with the change of operation point [17]. This stimulates the application of nonlinear control such as multivariable feedback linearization scheme (MFLC) to deal with the strong coupling and nonlinearities of the SG with FES [16], [17]. Although MFLC can provide global optimal performance over a wide range of operating points, this approach requires accurate system model and thus suffers from a complex control law and weak robustness to parameter uncertainties and external disturbances [18]. Many control methods have been purposed to address those drawbacks of the MFLC. Among them, one effective control method called perturbation estimation and compensation based nonlinear adaptive control (NAC) is proposed to enhance controller robustness and reduce model dependence, and applied to enhance power system stability, wind power generation and integration [19], [20], [21], [22], [23].

This paper investigates a perturbation compensation based NAC for synchronous generator (SG) with a FES and aims at a fully decoupled and robust control of rotor angle and terminal voltage, with fully confederation of model nonlinearities, model uncertainties, and external disturbance. Via defining lumped perturbation terms to include all unknown system nonlinearities, coupling between two loops, parameter uncertainties, and external disturbance, and designing two perturbation observers to estimate the perturbations, the NAC compensates the real perturbation by their estimates and achieve adaptive feedback linearization control without accurate system model. Two NAC strategies, state-feedback and output-feedback are investigated, respectively. Assuming all states are measure able and available, state-feedback based NAC is designed based on two perturbation observers (POs) for the terminal voltage loop and the rotor angle loop. The output-feedback NAC employs the voltage PO and designs state and perturbation observer (SPO) for the rotor angle loop to estimate states and perturbation terms of the rotor angle loop. The effectiveness of the proposed NAC schemes for the single bus infinite bus with FES (SMIB-FES) is verified via simulation studies and comparison with the MFLC. Moreover, the effectiveness of the SG with FES is also demonstrated by SG with the static excitation system controlled by PSS and AVR, respectively.

Main contributions of this paper are summarised as follows:

- The proposed NAC scheme employs perturbation estimation and compensation to achieve a fully decoupled control of the rotor angle and terminal voltage loops, and thus an enhanced control performance of SG with FES, i.e. using two control variables the equivalent compensated admittance and the excitation field voltage to achieve the decoupled control of two objectives: terminal voltage and rotor angle.
- Compared to linear control schemes derived and optimized based on operating point [13], [14], [15], the proposed NAC scheme can achieve a global optimal control performance over the entire operating range by fully considering all nonlinearities, and unmodeled system dynamics.
- With the estimation and compensation of the lumped perturbation term, the proposed NAC scheme doesn't require accurate system model and can achieve better robustness and simpler control law than the MFLC [17].
- The proposed output-feedback NAC doesn't require the full states feedback and can be easily extended to the multi-machine power system.

The remaining parts of this paper are organised as follows. Section II presents problem formulation. In Section III, the design of MFLC and NAC are presented. Section IV carries out the small signal stability analysis and simulation verification, compared with the AVR/PSS for SMIB with the conventional excitation system and the MFLC for SMIB-FES. Section V concludes this paper.

II. Problem Formulation

The topology diagram of a VSC-Chopper based FES proposed in [9] is shown in Fig.1. The main function of the front-end VSC is to maintain a constant DC capacitor voltage and then the field voltage can be controlled by the chopper only. Moreover, the front-end VSC can exchange reactive power with the generator terminal. Thus FES cannot only provide similar field voltage control like the conventional static excitation system, but also owns one more control input by adjusting reactive power exchange and controlling the generator terminal voltage.

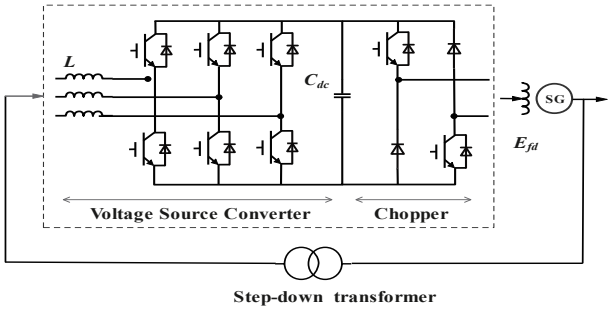

Fig. 1: Topology of a VSC and Chopper based FES

To simplify the analysis, the VSC and chopper in FES are assumed to be properly controlled to output the reference field voltage and reactive power fast enough, and thus, their dynamics are ignored [24]. The dynamic model of the VSC is ignored, and the exchange of reactive power with the grid is equivalent to compensating the shunt admittance b_{VSC} and simplified as a first-order system as in [17]:

$$\dot{b}_{VSC} = \frac{1}{T_Q}\left(-b_{VSC} + b^*_{VSC}\right) \tag{1}$$

where b^*_{VSC} is the reference of b_{VSC} and T_Q is the time constant of FES.

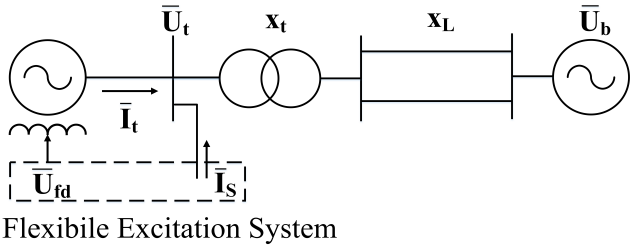

Fig. 2: SMIB including SG with a Flexible Excitation System

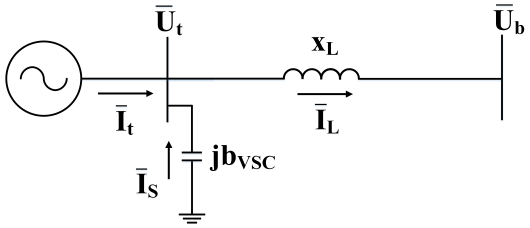

Fig. 3: Equivalent diagram of the SMIB with the FES

Fig.2 shows the configuration of a SMIB with SG installed with the FES. The equivalent diagram of the SMIB-FES is simplified in Fig. 3, considering the effect of the equivalent shunt admittance. From Fig.3, it can have

$$\begin{aligned} \bar{I}_L &= \bar{I}_t + \bar{I}_s = \bar{I}_t + jb_{VSC}\bar{U}_t \\ \bar{U}_t &= jx_L\bar{I}_L + \bar{U}_b = jx_L\bar{I}_t - x_L b_{VSC}\bar{U}_t + \bar{U}_b \end{aligned} \tag{2}$$

From equation (2), it can be obtained that

$$\bar{U}_t = \frac{jx_L\bar{I}_t + \bar{U}_b}{1 + x_L b_{VSC}} = jx_{l\Sigma}\bar{I}_t + \frac{\bar{U}_b}{c_{VSC}} \tag{3}$$

where $c_{VSC} = 1 + x_L b_{VSC}$ and $x_{l\Sigma} = x_L/c_{VSC}$.

The equivalent system is of a line impedance $x_{l\Sigma}$ connected to an infinite bus with a voltage being $\frac{U_b}{c_{VSC}}$. Therefore, with the equivalent shunt admittance (1), the mathematical model of the SMIB power system installed with the FES can be obtained by replacing x_L and U_b in the system with conventional excitation system by $x_{l\Sigma}$ and $\frac{U_b}{c_{VSC}}$, respectively [25].

$$\begin{cases} \dot{\delta} = \omega_0(\omega - 1) \\ \dot{\omega} = \frac{1}{T_j}\left(P_m - P_t - D(\omega - 1)\right) \\ \dot{E}'_q = \frac{1}{T'_{d0}}\left(E_{fd} - E_q\right) \\ \dot{b}_{VSC} = \frac{1}{T_Q}\left(-b_{VSC} + b^*_{VSC}\right) \end{cases} \tag{4}$$

$$\begin{cases} P_t = \frac{E'_q U_b}{c_{VSC}x'_{d\Sigma}}\sin\delta - \frac{U_b^2}{2c_{VSC}^2}\frac{(x_q - x'_d)}{x'_{d\Sigma}x_{q\Sigma}}\sin 2\delta \\ E_q = \frac{E'_q x_{d\Sigma}}{x'_{d\Sigma}} - \frac{(x_d - x'_d)U_b\cos\delta}{c_{VSC}x'_{d\Sigma}} \\ v_{td} = \frac{x_q U_b\sin\delta}{c_{VSC}x_{q\Sigma}}, \quad v_{tq} = \frac{x_{l\Sigma}E'_q}{x'_{d\Sigma}} + \frac{U_b x'_d\cos\delta}{c_{VSC}x'_{d\Sigma}} \\ U_t = \sqrt{v_{td}^2 + v_{tq}^2} \\ x'_{d\Sigma} = x'_d + x_{l\Sigma}, x_{d\Sigma} = x_d + x_{l\Sigma}, x_{q\Sigma} = x_q + x_{l\Sigma} \end{cases} \tag{5}$$

III. Design of perturbation observer-based nonlinear adaptive controller

This section firstly obtains the input-output relationship of the SMIB-FES. Then model-based MFLC [17] will be recalled, followed by the design of perturbation observers and the NAC for the voltage and the rotor angle loops, respectively.

A. Input-output representation

The multi-input multi-output (MIMO) system defined by (4)(5) can be expressed in the classical form of nonlinear system (6) for the design of the input–output feedback linearization control law of the SMIB-FES [16].

$$\begin{cases} \dot{X} = f(x) + g_1 u_1 + g_2 u_2 \\ y_1 = U_t \\ y_2 = \delta \end{cases} \tag{6}$$

where X are the state vector; y_1 and y_2 are the system outputs U_t and δ, respectively; u_1, u_2 are the inputs of the nonlinear FES.

$$X = \begin{bmatrix} \delta & \omega & E'_q & b_{VSC} \end{bmatrix}^T \tag{7}$$

$$u_1 = E_{fd} \tag{8}$$

$$u_2 = b^*_{VSC} \tag{9}$$

$$g_1 = \begin{bmatrix} 0 & 0 & \frac{1}{T'_{d0}} & 0 \end{bmatrix}^T \tag{10}$$

$$g_2 = \begin{bmatrix} 0 & 0 & 0 & \frac{1}{T_Q} \end{bmatrix}^T \tag{11}$$

The outputs y_1 and y_2 are indirectly related to the input u_1 and u_2 through the state variables and the nonlinear state equation. Therefore, an approach to build the explicit relationship between inputs and outputs is to differentiate the output y of the system until the inputs appear, thereby obtaining accurate input-output feedback linearization of the MIMO system. By means of calculating the Lie derivative for each output, the explicit relationship between inputs and outputs in (6) can be represented as

$$\begin{bmatrix} \dot{y}_1 \\ \dddot{y}_2 \end{bmatrix} = \begin{bmatrix} L_f y_1(X) \\ L_f^3 y_2(X) \end{bmatrix} + B(x)\begin{bmatrix} u_1 \\ u_2 \end{bmatrix} \tag{12}$$

$$B(x) = \begin{bmatrix} \beta_{11} & \beta_{12} \\ \beta_{21} & \beta_{22} \end{bmatrix} = \begin{bmatrix} L_{g_1} y_1(X) & L_{g_2} y_1(X) \\ L_{g_1} L_f^2 y_2(X) & L_{g_2} L_f^2 y_2(X) \end{bmatrix} \tag{13}$$

where $L_f y_1$, $L_f^3 y_2$ and components of $B(x)$ are Lie derivatives and can be found in Appendix A. The relative degree of outputs y_1 and y_2 are $r_1 = 1$ and $r_2 = 3$, respectively. The relative degree of the MIMO nonlinear system is $r = r_1 + r_2 = 4$, which equals to the system order and thus no internal dynamics needed to discussed.

B. Multi-variable FLC

As $B(x)$ is nonsingular in all operating range, the feedback control law can be designed to achieve the tracking control of U_t, δ with references U_t^*, δ^* as

$$\begin{bmatrix} u_1 \\ u_2 \end{bmatrix} = B(x)^{-1}\left(-\begin{bmatrix} L_f y_1 \\ L_f^3 y_2 \end{bmatrix} + \begin{bmatrix} v_1 \\ v_2 \end{bmatrix}\right) \tag{14}$$

$$\begin{aligned} v_1 &= \dot{y}_1^* + k_{11}e_1 \\ v_2 &= \dddot{y}_2^* + k_{21}\ddot{e}_2 + k_{22}\dot{e}_2 + k_{23}e_2 \end{aligned} \tag{15}$$

where $\begin{bmatrix} v_1 & v_2 \end{bmatrix}^T$ are linear control law; k_{11}, k_{21}, k_{22} and k_{23} are gains of linear controller; $e_1 = y_1^* - y_1$ and $e_2 = y_2^* - y_2$ are tracking errors.

The original system (12) is linearized as

$$\begin{bmatrix} \dot{y}_1 \\ \dddot{y}_2 \end{bmatrix} = \begin{bmatrix} v_1 \\ v_2 \end{bmatrix} \tag{16}$$

C. Perturbation Observers

Assume all nonlinearities of the system (12) are unknown, and define perturbation terms as

$$\begin{bmatrix} \Psi_1 \\ \Psi_2 \end{bmatrix} = \begin{bmatrix} L_f y_1(X) \\ L_f^3 y_2(X) \end{bmatrix} + (B(x) - B_0)\begin{bmatrix} u_1 \\ u_2 \end{bmatrix} \tag{17}$$

where Ψ_1 and Ψ_2 are the perturbation terms that contains all types of uncertainties and nonlinearities, $B_0 = B(x)|_{x=x(0)}$ is the nominal control gain. Then, (12) can be rewritten as

$$\begin{bmatrix} \dot{y}_1 \\ \dddot{y}_2 \end{bmatrix} = \begin{bmatrix} \Psi_1 \\ \Psi_2 \end{bmatrix} + B_0(x)\begin{bmatrix} u_1 \\ u_2 \end{bmatrix} \tag{18}$$

Defining state variables as $z_{11} = y_1$, $z_{21} = y_2, z_{22} = \dot{y}_2, z_{23} = \ddot{y}_2$, and two fictitious states to represent perturbation terms as $z_{12} = \Psi_1(x)$ and $z_{24} = \Psi_2(x)$, two extended-order subsystems are given by

$$\begin{cases} \dot{z}_{11} = z_{12} + \beta_{11_0}u_1 + \beta_{12_0}u_2 \\ \dot{z}_{12} = \dot{\Psi}_1 \end{cases} \tag{19}$$

$$\begin{cases} \dot{z}_{21} = z_{22} \\ \dot{z}_{22} = z_{23} \\ \dot{z}_{23} = z_{24} + \beta_{21_0}u_1 + \beta_{22_0}u_2 \\ \dot{z}_{24} = \dot{\Psi}_2 \end{cases} \tag{20}$$

When all system states are available, two second-order POs can be designed to estimate the perturbations Ψ_1 and Ψ_2, using system outputs $y_1 =$ and $y_3 = z_{23} = \ddot{\delta}$ as shown in (21) and (22). Note that the terminal voltage y_1 is a measurable output, but the output $y_3 = \ddot{\delta}$ should be calculated from available measurements based on (4) or replaced by other available measurements such as the active power P_t for easy implementation.

PO for voltage loop:

$$\begin{cases} \dot{\hat{z}}_{\mathrm{PO11}} = \hat{z}_{\mathrm{PO12}} + l_{11}\left(y_1 - \hat{z}_{\mathrm{PO11}}\right) + \beta_{11_0}u_1 + \beta_{12_0}u_2 \\ \dot{\hat{z}}_{\mathrm{PO12}} = l_{12}\left(y_1 - \hat{z}_{\mathrm{PO11}}\right) \end{cases} \tag{21}$$

PO for rotor angle loop:

$$\begin{cases} \dot{\hat{z}}_{\mathrm{PO23}} = \hat{z}_{24} + l_{31}\left(y_3 - z_{\mathrm{PO23}}\right) + \beta_{21_0}u_1 + \beta_{22_0}u_2 \\ \dot{\hat{z}}_{\mathrm{PO24}} = l_{32}\left(y_3 - \hat{z}_{\mathrm{PO23}}\right) \end{cases} \tag{22}$$

where $\hat{z}_{\mathrm{PO}ij}$ are the estimates of z_{ij}, and l_{ij} are observer gains which can be chosen by the pole placement technique.

When only system outputs are available, a fourth-order SPO can be designed to estimate the states $\dot{\delta}, \ddot{\delta}$ and the perturbations Ψ_2 by using system output $y_2 = \delta$ instead of $y_3 = \ddot{\delta}$ as shown in (23).

SPO for rotor angle loop:

$$\begin{cases} \dot{\hat{z}}_{21} = \hat{z}_{22} + l_{21}\left(y_2 - \hat{z}_{21}\right) \\ \dot{\hat{z}}_{22} = \hat{z}_{23} + l_{22}\left(y_2 - \hat{z}_{21}\right) \\ \dot{\hat{z}}_{23} = \hat{z}_{24} + l_{23}\left(y_2 - \hat{z}_{21}\right) + \beta_{21_0}u_1 + \beta_{22_0}u_2 \\ \dot{\hat{z}}_{24} = l_{24}\left(y_2 - \hat{z}_{21}\right) \end{cases} \tag{23}$$

where $\hat{z}_{ij}$ are the estimates of z_{ij}. The diagram of PO (21) and SPO (23) are shown in Fig. 4.

D. Nonlinear Adaptive Controller Design

By cancelling the real system perturbation with their estimates, state-feedback and output-feedback based NACs can be designed based on the POs and SPOs, respectively. The state-feedback based NAC can be obtained as:

$$\begin{bmatrix} u_1 \\ u_2 \end{bmatrix} = B_0^{-1}\left(-\begin{bmatrix} \hat{z}_{\mathrm{PO12}}(x) \\ \hat{z}_{\mathrm{PO32}}(x) \end{bmatrix} + \begin{bmatrix} v_1 \\ v_2 \end{bmatrix}\right) \tag{24}$$

$$\begin{aligned} v_1 &= \dot{y}_1^* + k_{11}(y_1^* - y_1) \\ v_2 &= \dddot{y}_2^* + k_{21}(\ddot{\delta}^* - \ddot{\delta}) + k_{22}[\dot{\delta}^* - \dot{\delta}] + k_{23}(\delta^* - \delta) \end{aligned} \tag{25}$$

For the output-feedback based NAC, the PO (21) and SPO (23) will estimate the system perturbation Ψ_1 and Ψ_2 and the states $\dot{\delta}, \ddot{\delta}$. The output-feedback based NAC for the system can be expressed as

$$\begin{bmatrix} u_1 \\ u_2 \end{bmatrix} = B_0^{-1}\left(-\begin{bmatrix} \hat{z}_{\mathrm{PO12}}(x) \\ \hat{z}_{24}(x) \end{bmatrix} + \begin{bmatrix} v_1 \\ v_2 \end{bmatrix}\right) \tag{26}$$

$$\begin{aligned} v_1 &= \dot{y}_1^* + k_{11}(y_1^* - y_1) \\ v_2 &= \dddot{y}_2^* + k_{21}(\ddot{\delta}^* - \hat{z}_{23}) + k_{22}[\dot{\delta}^* - \hat{z}_{22}] + k_{23}(\delta^* - \delta) \end{aligned} \tag{27}$$

The block diagram of the output-feedback NAC is shown in Fig. 4. The implementation of the proposed control scheme only requires the measurement of the terminal voltage and rotor angle. With proper observer gains, the designed perturbation observers can actively estimate the time-varying perturbation using the measured outputs y_1 and y_2. Compared with the MFLC proposed in [17], the proposed controller doesn't requires the detailed model and full state measurements but all nonlinearities together with external disturbances are still be considered. Note that the stability analysis of the closed-loop system formed of the plant (4)-(5), the perturbation observer (21)-(22), and the controller (24) is presented in Appendix B.

The flowchart of the output-feedback NAC is shown in Fig. 5. The designed perturbation observers (21) and (23), feeding by the measured outputs y_1 and y_2, can estimate the states $\dot{\delta}$, $\ddot{\delta}$, and system perturbation Ψ_1 and Ψ_2. With the measured outputs, estimated states and system perturbation, the proposed output-feedback NAC can regulate the terminal voltage and power angle stability by adjusting the field voltage and compensating equivalent admittance.

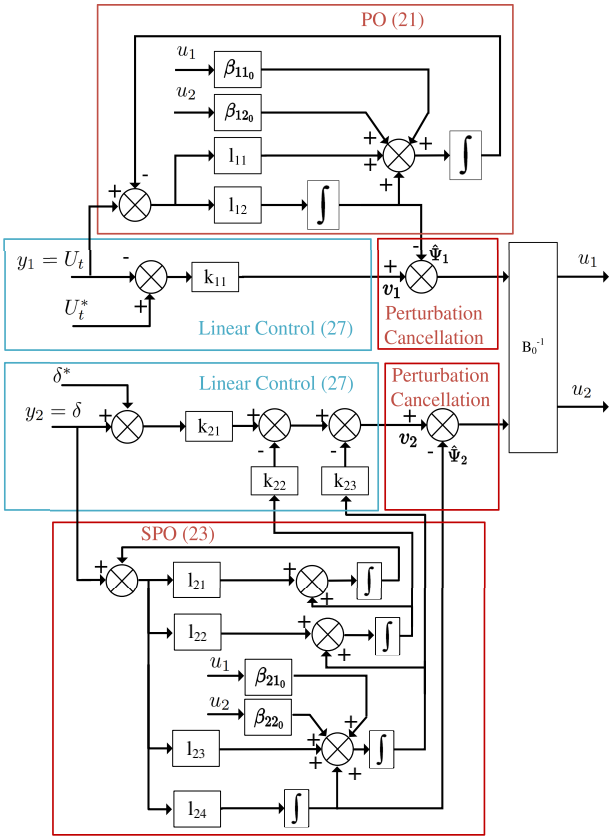

Fig. 4: Block diagram of the proposed output-feedback NAC with SPOs

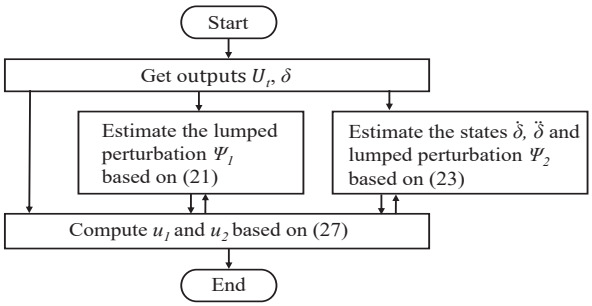

Fig. 5: Flowchart of the proposed output-feedback NAC with SPOs

IV. Simulation Results

The proposed controllers have been tested via small-signal stability analysis and simulation in MATLAB/Simulink. The control performance of the proposed controllers is compared with the performance of the MFLC [17] and the AVR+PSS for the conventional excitation system [26]. The inputs of the AVR+PSS are the deviation of rotor speed and the terminal voltage, and the MFLC requires full state feedback. Due to the similar performance of state-feedback and output-feedback based NAC, only results of the output-feedback NAC are presented.

Parameters of SMIB shown in Fig.3 are given in Table I. The control inputs are bounded as $|u_1| \leq 5$ p.u. and $|u_2| \leq 0.1$ p.u. Parameters of the NACs are designed based on pole placement method and listed as following: POs: $l_{11} = 1 \times 10^3$, $l_{12} = 2.5 \times 10^5$, $l_{31} = 1.28 \times 10^3$, $l_{32} = 4.096 \times 10^5$, SPO: $l_{21} = 4.4 \times 10^3$, $l_{22} = 7.26 \times 10^6$, $l_{23} = 5.324 \times 10^9$, $l_{24} = 1.4641 \times 10^{12}$ Controller: $k_{11} = 2$, $k_{21} = 6$, $k_{22} = 24$, $k_{21} = 16$. Note that MFLC uses same controller parameters as the NAC.

TABLE I: Parameters of SMIB with the FES

d-axis synchronous reactance	x_d	1.2
q-axis synchronous reactance	x_q	0.3
d-axis transient reactance	x'_d	0.3
Line reactance	x_L	0.2
Nominal synchronous speed	w_0	$2\pi f$
Rotor inertia constant	T_j	9.48
d-axis OC transient time constant	T'_{do}	5.9
Mechanical input power	P_m	1
Damping	D	0.1
Bus voltage	U_b	1
Reactive power regulator time constant	T_Q	0.1

All in per unit except that T_j, T'_{d0} and T_Q are in second.

A. Small-signal Stability Analysis and Verification

Results of small-signal stability analysis of the SMIB-FES is shown in Table II which gives eigenvalues, oscillation frequency and damping ratio (ζ) of dominate poles. It indicates that both MFLC and proposed NAC can ensure damping performance under different operation points, while damping ratio of the linear control (AVR+PSS) changes with the operation point. Moreover, FES can provide better damping performance than the conventional static excitation system, though results of FES with linear control is not presented in this paper [13].

TABLE II: Small-signal stability of SMIB with FES

Operating Point	Controller Type	Eigenvalue	Frequency	ζ
$P_m = 1.00$	AVR+PSS	$-1.6578 \pm 9.0773i$	1.2855	0.2010
	MFLC	$-0.8861 \pm 0.4223i$	0.0672	0.9027
	NAC	$-0.8201 \pm 0.5136i$	0.0817	0.8475
$P_m = 0.60$	AVR+PSS	$-1.3911 \pm 8.4715i$	1.3483	0.1620
	MFLC	$-0.8861 \pm 0.4223i$	0.0672	0.9027
	NAC	$-0.8528 \pm 0.4702i$	0.0840	0.8369

Simulation verification under small disturbance are given in Fig. 6-8. 3% step change of the reference terminal voltage is applied at $2s$. The simulation results are shown in Fig. 6-8. Fig.6 compares the control performance of FES under different control and the results of a thyristor excitation system controlled by conventional controller AVR+PSS. Both MFLC and NAC can track the variation of terminal voltage reference immediately. In Fig.6, under the NAC control of FES, the steady time is 5 s , while those under AVR+PSS control is 6 s. Therefore, it is obvious that the NAC and MFLC is more effective in improving the small-signal stability of the power system.

The effectiveness of NAC is verified considering the change of operation point of the SMIB-FES. In this scenario, additional 5% input mechanical power is added at $1s$. The results are compared with the SMIB with AVR+PSS and the SMIB-FES with MFLC as shown in Fig. 9-12. In Fig. 9 and Fig. 10, MFLC and NAC show less overshoot and oscillation compared

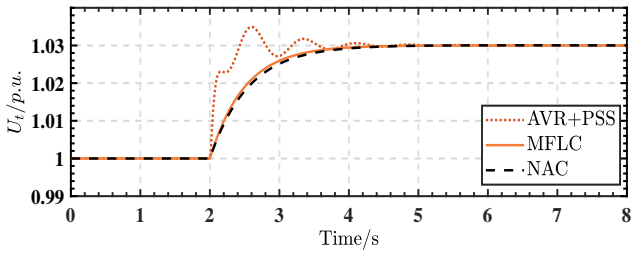

Fig. 6: Terminal voltage response under a $+3\%$ step change of the voltage reference

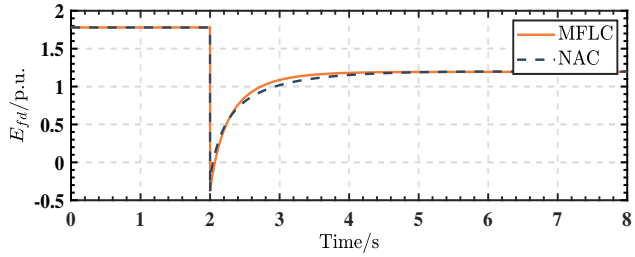

Fig. 7: Filed voltage response under a $+3\%$ step change of the voltage reference

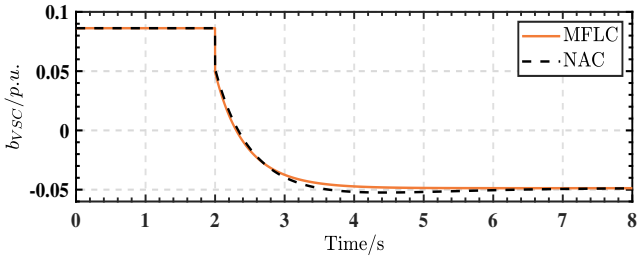

Fig. 8: Equivalent compensated admittance response under a $+3\%$ step change of the voltage reference

with AVR+PSS. The response of field voltage and equivalent compensated admittance to the change of operation point are given in the Fig. 11 and Fig. 12.

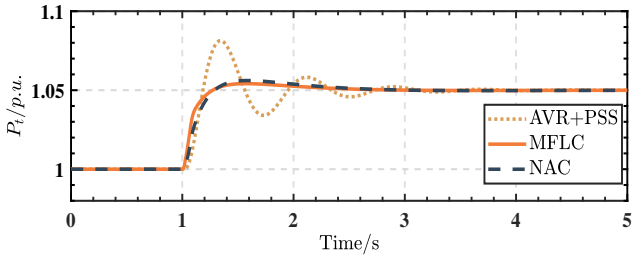

Fig. 9: Electrical power response under operation point change

B. Three-Phase Short Circuit Fault Response

The fault is simulated as: a three-phase short circuit occurs at the end of the line near the infinite bus and lasts $0.1s$. System responses with proposed control scheme installed on

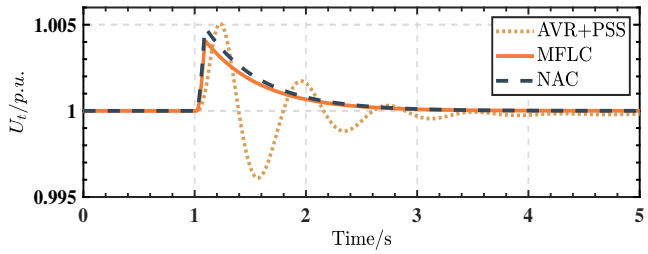

Fig. 10: Terminal voltage response under operation point change

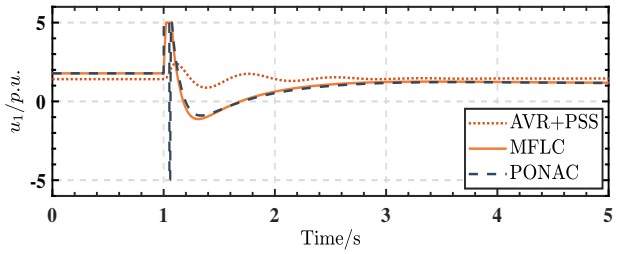

Fig. 11: Field voltage response under operation point change

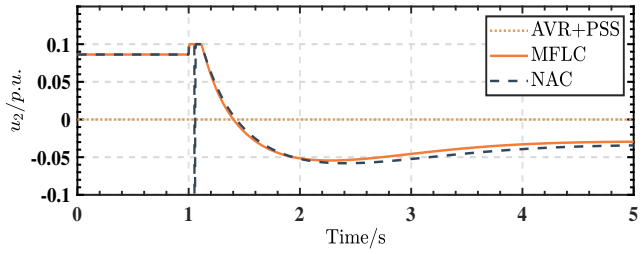

Fig. 12: Equivalent compensated admittance response under operation point change

the SMIB under the operation condition, are shown in Fig. 13. The control inputs are shown in Fig. 14. To illustrate the similar control performance of state-feedback and output-feedback based NACs, the results are presented by PONAC and SPONAC, respectively.

Results demonstrate that the oscillation of terminal voltage is better damped with MFLC and NAC compared with AVR+PSS. For the dynamic of rotor angle and rotor speed shown in Fig. 13(b), (c), the transient process with NAC control is shorter than that of AVR+PSS control. These results illustrate that the output-feedback NAC scheme can provide as good control performance as that of MFLC due to the fast online estimation.

The tiny difference of control performance between MFLC and the proposed NAC is due to the estimation error of the PO and the SPO. The observer performance is shown in Fig.15-16, which illustrates that the observer can provide accurate estimation of these lumped perturbation when the system suffers three-phase short circuit fault. Note that there exists a dramatic change at the instant when the faults occur in the power system, the estimation error soars immediately when the fault occurs and disappears at $t = 1s$ and $t = 1.1s$. The

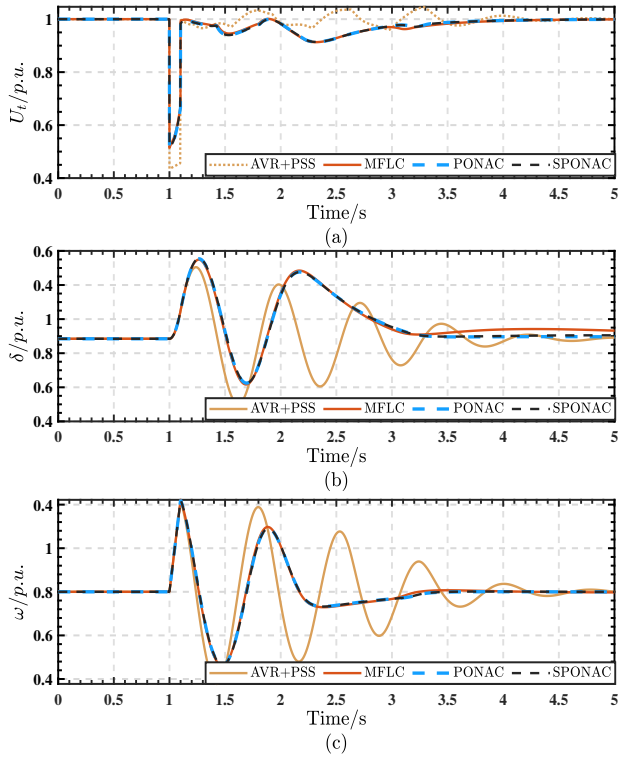

Fig. 13: Responses under three-phase short circuit fault: (a) terminal voltage, (b) rotor angle, (c) rotor speed.

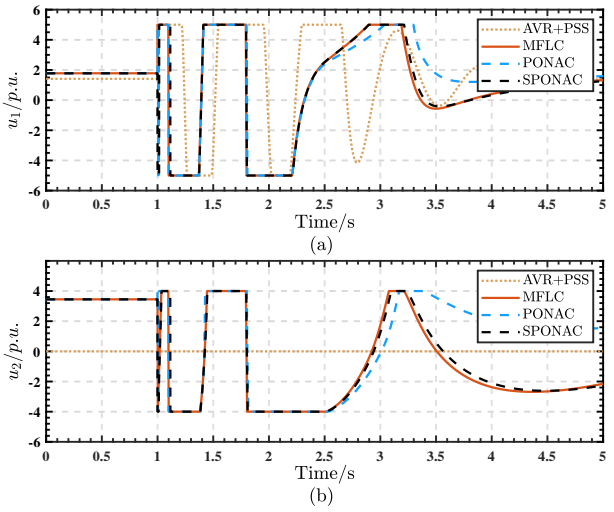

Fig. 14: Control inputs under a three-phase short-circuit fault: (a) field voltage, (b) equivalent compensated admittance.

PO and SPO cannot deal with the discontinuity of the states very well at this specific instant. However, from the estimation error results shown in Fig.15-16, one can see that the observer is able to provide accurate state estimates with a fast track after fault. despite of the state discontinuity.

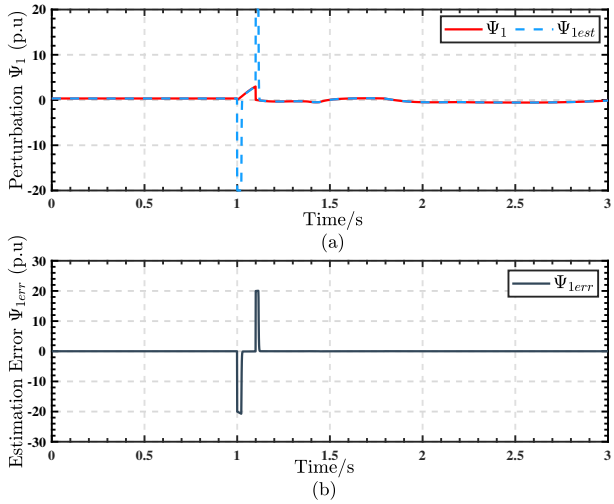

Fig. 15: Estimation error of PO for Perturbation Ψ_1: (a) Ψ_1, (b) Ψ_{1err}.

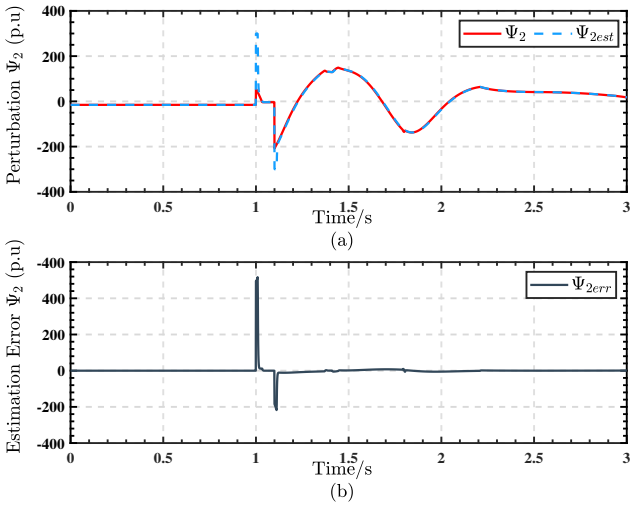

Fig. 16: Estimation error of SPO for Perturbation Ψ_2: (a) Ψ_2, (b) Ψ_{2err}.

C. Robustness Against Parameter Uncertainties

Note that the accurate SG parameters are usually difficult to obtain as their values might be affected by the ambient environment temperature, wear-and-tear, generator ageing and measurement error, so the use of their nominal value in the controller loop can result in an inaccurate response [27]. In order to test the robustness of proposed controller, a 10% increase of the inertia constants T_J and the field time constant T'_{do} of the SG from its nominal values is tested. Meanwhile, a three-phase short circuit happens at $t = 1s$ and lasts $0.1s$.

The corresponding system responses of AVR+PSS, MFLC and the proposed NAC are given by Fig.17-19. One can be seen that MFLC cannot track the reference signal U_t^* and δ^* as it requires an accurate system model. Therefore, when suffering parameters uncertainties during the design of MFLC, MFLC cannot maintain its control performance in practice. In contrast, the proposed state-feedback control based on PO and SPO can provide a great robustness to SMIB-FES in the presence of system uncertainties. When inertia constants and field time constant are mismatched with the nominal value, the PO and SPO are able to estimate fast time-varying disturbances to assist excitation system, thereby maintaining rotor angle and terminal voltage.

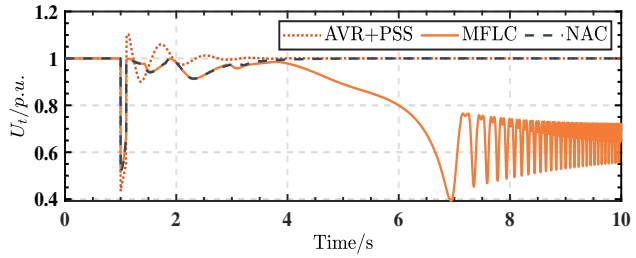

Fig. 17: Terminal voltage response under parameter uncertainties and three-phase short circuit fault

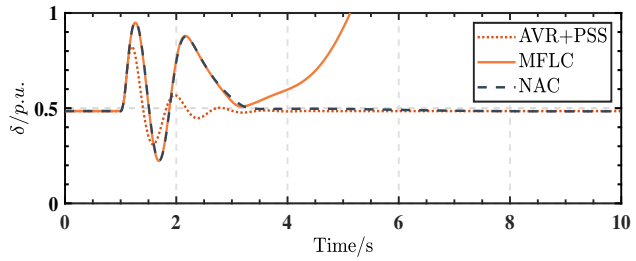

Fig. 18: Rotor angle response under parameter uncertainties and three-phase short circuit fault

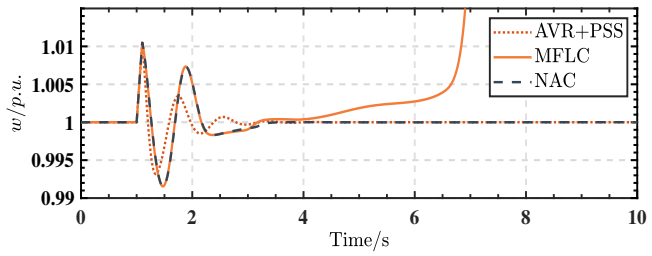

Fig. 19: Rotor speed response under parameter uncertainties and three-phase short circuit fault

V. Conclusion

In this paper, NAC schemes have been proposed for SG with FES in a SMIB, based on perturbation estimation and compensation in adaptive feedback linearization control. FES using fully controlled devices can provide simultaneously regulation of terminal voltage, and rotor angle via controlling field voltage and equivalent compensated admittance. After obtaining the input-output linearization relationship between two outputs and two inputs, perturbation observers are designed to estimate the lumped perturbation including all uncertainties and time-varying nonlinearities and external disturbances. By using the estimated perturbations to compensate their real value, the proposed NAC schemes are achieved without requiring the detailed system model, resulting in simpler implementation and better robustness than the model-based MFLC. The proposed nonlinear control can provide a global optimal performance across the whole operation region. Moreover, output-feedback control is obtained by deigning SPOs for the rotor angle loop. The small-signal stability analysis shows that FES can provide better damping performance than the conventional static excitation system, and the nonlinear NAC and MFLC with better damping than the linear AVR+PSS. Simulation verification and comparison among AVR+PSS, MFLC and NAC shows that the proposed NAC has superior damping performance and better robustness. Further studies will focus on investigating NAC scheme on multi-machine power system and partial feedback linearization by replacing rotor angle with easily measured variables.

References

[1] Vittal, V., McCalley, J.D., Anderson, P.M. et al.: 'Power system control and stability', (Wiley Wiley-IEEE Press, USA, 2019, 3rd edn.)

[2] Fan, B., Yang, Q., Wang, K., Xu, J., et al: 'Transient stability enhancement control of power systems with time-varying constraints', *IET Gener. Transm. Distrib*, 2016, 10, 3251-3270(2016)

[3] Kundur, P., Balu, N.J., Lauby, M.G.: 'Power system stability and control', (McGraw-Hill, New York, 1994, 1st edn.)

[4] Nøland, J.K., Evestedt, F., Perez-Loya, J.J., et al: 'Comparison of thyristor rectifier configurations for a six-phase rotating brushless outer pole PM exciter', *IEEE Trans. Ind. Electron*, 65, 968–976(2018)

[5] Hughes, F.M., Lara, O.A., Jenkins, N., and Strbac G.: 'A power system stabilizer for DFIG-based wind generation', *IEEE Trans. Power Syst*, 21, 763–772(2006)

[6] Johnson, S. C., Rhodes, D. J., Webber, E, M.: 'Understanding the impact of non-synchronous wind and solar generation on grid stability and identifying mitigation pathways', *Appl. Energy*, 262, 1-11(2020)

[7] Paital, S.R., Ray, P.K., Mohanty, A.: 'Comprehensive review on enhancement of stability in multimachine power system with conventional and distributed generations', *IET Renew. Power Gener*, 12, 1854–1863(2018)

[8] Nøland, J.K., Nuzzo, S., Tessarolo, A., et al: 'Excitation System Technologies for Wound-Field Synchronous Machines: Survey of Solutions and Evolving Trends', *IEEE ACCESS*, 7, 109699 - 109718(2019)

[9] Yang, J., Chen, Z., Mao, C., et al: 'Analysis and assessment of VSC excitation system for power system stability enhancement', *Int. J. Elect. Power Energy Syst*, 57, 350-357(2014)

[10] Yao, K., Ruan, X., Zou, C., et al: 'Three-phase single-switch boost power factor correction converter with high input power factor' *IET Power Electron*, 5, 1095 – 1103(2012)

[11] Singh, B., Singh, B.N., Chandra, A., et al: 'A review of three-phase improved power quality AC-DC converters', *IEEE Trans. Ind. Electron*, 51, 641-660(2004)

[12] Lee, W.C., Hyun, D.S., Lee, T.K.: 'A novel control method for three-phase PWM rectifiers using a single current sensor', *IEEE Trans. Power Electron*, 15, 861–870(2000)

[13] Chen, Z., Mao, C., Wang, D., et al: 'Design and implementation of voltage source converter excitation system to improve power system stability', *IEEE Trans. Ind. Appl*, 52, 2778-2788(2016)

[14] Zhou, Y., Mao, C., Chen, Z., et al: 'A novel control strategy for static excitation system based on three-phase current source converter', *Proc. 5th Int. Conf. Electr. Utility Deregulation Restructuring Power Technol*, 57, 1240-1245(2015)

[15] Zhang, T., Mao, C., Zhang, J., et al: 'Design and field application of flexible excitation system damping controllers', *IEEE Trans. Ind. Electron*, 68, 949-959(2021)

[16] Slotine, J.E., Slotine, J., Li, W: 'Applied nonlinear control', (Prentison-Hall, USA, 1988, 1st edn.)

[17] Mao, C., He, J., Wang, D., et al: 'Multivariable feedback linearization scheme for new excitation systems based on full controlled device', *Proc. CSEE*, 36, 53–60(2013)

[18] Khalil, H.K: 'Nonlinear systems', (Prentison-Hall, USA, 2002, 3rd edn.)

[19] Jiang, L., Wu, Q., Wen, J : 'Decentralized nonlinear adaptive control for multimachine power systems via high-gain perturbation observer', *IEEE Trans. Circuit Syst. I Regul. Paper*, 51, 2052-2059(2004)

[20] Roy, T,K., Mahud, M.A., Shen, W., et al: 'A non-linear adaptive excitation control scheme for feedback linearized synchronous generations in multimachine power systems', *IET Gener. Transm. Distrib*, 15, 1501-1520(2021)

[21] Yan, L., Chen, X., Zhou, X., et al: 'Perturbation compensation-based non-linear adaptive control of ESS-DVR for the LVRT capability improvement of wind farms', *IET Renew. Power Gener*, 12, 1500–1507(2018)

[22] Shi, K., Yin, X., Jiang, L et al: 'Perturbation estimation based nonlinear adaptive power decoupling control for dfig wind turbine', *IEEE Trans. Power Electron*, 35, 319-333(2019)

[23] Chen, J., Yao, W., Zhang, C., et al: 'Design of robust MPPT controller for grid-connected PMSG-Based wind turbine via perturbation observation based nonlinear adaptive control', *Renew. Energy*, 134, 478-495(2019)

[24] Rodriguez, J.R., Dixon, J.W., Espinoza, J,R., et al: 'PWM regenerative rectifiers: state of the art', *IEEE Trans. Ind. Electron.* 52, 5-22(2005)

[25] Wang, H., Du, W: 'Analysis and damping control of power system low-frequency oscillations', (Springer, New York, USA, 2016)

[26] *IEEE Recommended Practice for Excitation System Models for Power System Stability Studies*, IEEE Standard 421.5-2016(2016)

[27] Lu, Q., Sun, Y., Mei, S: 'Nonlinear Control Systems and Power System Dynamics', (Academic Publishers, Boston, MA, USA, 2001)

APPENDIX A
LIE DERIVATIVE

$$
\begin{aligned}
L_f y_1 =& \frac{b_{VSC}}{T_Q}\left[\left(\frac{2E'_q x_L}{c_{VSC}x'_{d\Sigma}2^2}+\frac{2U_b x'_d\cos\delta}{x'_{d\Sigma}\left(b_{VSC}+1\right)}\right)\right.\\
&\left(\frac{E'_q x_L^2}{c_{VSC}^2 x'_{d\Sigma}}-\frac{E'_q x_L^3}{c_{VSC}^3 x'_{d\Sigma}}+\frac{U_b x'_d\cos\delta}{x'_{d\Sigma}\left(b_{VSC}+1\right)^2}\right.\\
&\left.\left.-\frac{x'_{d\Sigma}x_L^2U_b^2\cos\delta}{c_{VSC}^2x'_{d\Sigma}\left(b_{VSC}+1\right)}\right)+\frac{2x_d^2x_q^2\sin\delta^2}{x'_{q\Sigma}\left(b_{VSC}+1\right)^3}\right.\\
&\left.+\frac{2x_d^2x_q^2x_L^2\sin\delta^2}{c_{VSC}^2{x'_{q\Sigma}}^3\left(b_{VSC}+1\right)^2}\right]\\
&-\frac{\omega_0(\omega-1)\left[\frac{2U_bd(x)x'_d\sin\delta}{x'_{d\Sigma}(1+b_{VSC})}-\frac{2x_d^2x_q^2\cos\delta\sin\delta}{x_{q\Sigma}^2(b_{VSC}+1)^2}\right]}{2c(x)}\\
&-\frac{x_Ld(x)\left[\frac{x_{d\Sigma}E'_q}{x'_{d\Sigma}(1+b_{VSC})}+\frac{\left(x_d-x'_d\right)U_b\cos\delta}{x'_{d\Sigma}(b_{VSC}+1)}\right]}{T'_{d\rho}c_{VSC}x'_{d\Sigma}c(x)}
\end{aligned}
$$

$$
c(x)=\sqrt{\left(\frac{E'_qx_L}{c_{VSC}x'_{d\Sigma}}+\frac{U_bx'_dcos\delta}{x'_{d\Sigma}(b_{VSC}+1)}\right)^2+\frac{x_d^2x_q^2sin\delta^2}{x_{q\Sigma}^2(b_{VSC}+1)^2}}
$$

$$
\begin{aligned}
L_f^3 y_2 =& \frac{D\omega_0}{T_j^2}\left[D(\omega-1)-P_m+\frac{E'_qU_b\sin\delta}{x'_{d\Sigma}\left(b_{VSC}+1\right)}\right.\\
&\left.+\frac{U_b^2\left(x'_d-x_q\right)\sin2\delta}{2x'_{d\Sigma}x_{q\Sigma}\left(b_{VSC}+1\right)^2}\right]-\frac{\omega_0^2(\omega-1)}{T_j}\\
&\left[\frac{E'_qU_b\cos\delta}{x'_{d\Sigma}\left(b_{VSC}+1\right)}+\frac{\left(x'_d-x_q\right)U_b^2\cos2\delta}{x'_{d\Sigma}x_{q\Sigma}\left(b_{VSC}+1\right)^2}\right]\\
&+\frac{b_{VSC}\omega_0}{T_Q}\left[\frac{x_L^2E'_qU_b\sin\delta}{c_{VSC}x'_{d\Sigma}}-\frac{U_b^2\left(x'_d-x_q\right)\sin2\delta}{x'_{d\Sigma}x_{q\Sigma}\left(b_{VSC}+1\right)^3}\right.\\
&-\frac{E'_qU_b\sin\delta}{x'_{d\Sigma}\left(b_{VSC}+1\right)^2}+\frac{U_b^2x_L^2\left(x'_d-x_q\right)\sin2\delta}{2c_{VSC}^2x_{q\Sigma}^2x'_{d\Sigma}\left(b_{VSC}+1\right)^2}\\
&\left.+\frac{U_b^2x_L^2\left(x'_d-x_q\right)\sin2\delta}{2c_{VSC}^2{x'_{d\Sigma}}^2x_{q\Sigma}\left(b_{VSC}+1\right)^2}\right]+\left[\frac{E'_qx_{d\Sigma}}{x'_{d\Sigma}}\right.\\
&\left.-\frac{U_b\left(x_d-x'_d\right)\cos\delta}{x'_{d\Sigma}\left(b_{VSC}+1\right)}\right]\frac{U_b\omega_0\sin\delta}{T'_{do}T_jx'_{d\Sigma}\left(b_{VSC}+1\right)}
\end{aligned}
$$

$$
d(x)=\frac{E'_qx_L}{c_{VSC}x'_{d\Sigma}}+\frac{U_bx'_d\cos\delta}{x'_{d\Sigma}\left(b_{VSC}+1\right)}.
$$

$$
\beta_{11}=\frac{x_L[\frac{E'_qx_L}{c_{VSC}x'_{d\Sigma}}+\frac{U_bx'_dcos\delta}{x'_{d\Sigma}(b_{VSC}+1)}]}{T'_{do}c_{VSC}x'_{d\Sigma}c(x)}
$$

$$
\begin{aligned}
\beta_{12}=&-\frac{1}{2T_Qc(x)}[(\frac{2E'_qx_L}{c_{VSC}x'_d}+\frac{2U_bx'_dcos\delta}{x'_d(b_{VSC}+1)})\\
&(\frac{E'_qx_L^2}{{c_{VSC}}^2x'_{d\Sigma}}-\frac{E'_qx_L^2}{{c_{VSC}}^3{x'_{d\Sigma}}^2}+\frac{U_bx'_dcos\delta}{x'_{d\Sigma}(b_{VSC}+1)^2}\\
&-\frac{U_b{x'_d}^2cos\delta}{{c_{VSC}}^2x'_{d\Sigma}(b_{VSC}+1)}+\frac{2x_d^2x_q^2sin\delta^2}{x_{q\Sigma}^2(b_{VSC}+1)^3}\\
&-\frac{2x_L^2x_d^2x_q^2sin\delta^2}{{c_{VSC}}^2{x'_{d\Sigma}}^3(b_{VSC}+1)^2})]
\end{aligned}
$$

$$
\beta_{21}=-\frac{U_S\,w_0\,\sin\delta}{T'_{do}\,Tj\,x'_{d\Sigma}\left(b_{VSC}+1\right)}
$$

$$
\begin{aligned}
\beta_{22}=&-\frac{\omega_0}{T_QT_J}(\frac{E'_qU_bx_Lsin\delta}{{c_{VSC}}^2{x'_{d\Sigma}}^2(b_{VSC}+1)}\\
&-\frac{(x'_d-x_q){U_b}^2sin2\delta}{x'_{d\Sigma}x_{q\Sigma}(b_{VSC}+1)^3}-\frac{E'_qU_bsin\delta}{x'_{d\Sigma}(b_{VSC}+1)^2}\\
&+\frac{(x'_d-x_q)x_L^2U_b^2sin2\delta}{2{c_{VSC}}^2x'_{d\Sigma}{x_{q\Sigma}}^2(b_{VSC}+1)^2}\\
&+\frac{(x'_d-x_q)x_L^2U_b^2sin2\delta}{2{c_{VSC}}^2x'_{d\Sigma}x_{q\Sigma}(b_{VSC}+1)^2})
\end{aligned}
$$

APPENDIX B
STABILITY ANALYSIS OF CLOSED-LOOP SYSTEM

The stability of the closed-loop system formed of the plant (4)-(5), the perturbation observer (21)-(22), and the controller (24) are investigated in the appendix, based on the approach in [18], [19]. The stability of the closed-loop system including the observers (21), (23), and the controller (26) can be analysed using the method presented in the following section. For

convenience, the compact form of perturbation observers is written as

$$\begin{cases} \dot{\hat{z}}_{i1} = \hat{z}_{i2} + l_{11}\tilde{z}_i + \beta_{i1_0}u_1 + \beta_{i2_0}u_2 \\ \dot{\hat{z}}_{i2} = l_{12}\tilde{z}_i \end{cases} \tag{28}$$

where $\tilde{z}_i = z_i - \hat{z}_i$ is the estimation error of z_i.

Choosing

$$l_{i1} = \frac{\alpha_{i1}}{\epsilon_i}, l_{i2} = \frac{\alpha_{i2}}{\epsilon_i^2} \tag{29}$$

the scaled estimation errors can be represented as

$$\eta_{i1} = \frac{\tilde{z}_{i1}}{\epsilon_i} \quad \eta_{i2} = \tilde{z}_{i2} \tag{30}$$

Using the scaled estimation errors, the dynamics of the perturbation observer is

$$\epsilon_i \dot{\eta}_{po_i} = A_{po_i}\eta_{po_i} + \epsilon_i B_{po_i}\dot{\Psi}_i \tag{31}$$

where $\eta_{po_i} = [\eta_{i1} \quad \eta_{i2}]^T$,

$$A_{po_i} = \begin{bmatrix} -\alpha_{i1} & 1 \\ -\alpha_{i2} & 0 \end{bmatrix} \quad B_{po_i} = \begin{bmatrix} 0 \\ 1 \end{bmatrix} \tag{32}$$

The positive constants α_{i1} and α_{i2} are chosen such that A_{po_i} is a Hurwitz matrix, and ϵ_i, $0 < \epsilon_i \ll 1$, is a small positive constant to be specified. ϵ_i is chosen small enough to ensure that the dynamics of the estimation error will be much faster than that of the system (4)-(5).

Substitution of u_1 and u_2 in (24) into system (18) can obtain

$$\begin{cases} \dot{y}_1 = \dot{y}_1^* + k_{11}(y_1^* - y_1) + \eta_{12} \\ \ddot{y}_2 = \ddot{y}_2^* + k_{21}(\ddot{y}_2^* - \ddot{y}_2) + k_{22}(\dot{y}_2^* - \dot{y}_2) \\ \qquad + k_{23}(y_2^* - y_2) + \eta_{22} \end{cases} \tag{33}$$

Defining tracking errors as $e_1 = y_1^* - y_1$ and $e_2 = y_2^* - y_2$, the dynamic of tracking errors can be represented as

$$\begin{cases} \dot{e}_1 = -k_{11}e_1 + \eta_{12} \\ \ddot{e}_2 = -k_{21}\ddot{e}_2 + k_{22}\dot{e}_2 + k_{23}e_2 + \eta_{22} \end{cases} \tag{34}$$

then

$$\dot{e}_i = A_{i0}e_i + B_{i0}\eta_{i2} \tag{35}$$

where $i = 1, 2$, $B_{i0} = \begin{bmatrix} 1 & 0 & 0 & 1 \end{bmatrix}^{\mathrm{T}}$, and

$$A_{i0} = \begin{bmatrix} k_{11} & 0 & 0 & 0 \\ 0 & 0 & 1 & 0 \\ 0 & 0 & 0 & 1 \\ 0 & k_{21} & k_{22} & k_{23} \end{bmatrix}$$

Finally, the closed-loop system including the controller/perturbation observer can be represented as

$$\dot{e}_i = A_{i0}e_i + B_{i0}\eta_{i2} \tag{36}$$

$$\dot{\eta}_{po_i} = \frac{1}{\epsilon_i}A_{po_i}\eta_{po_i} + B_{po_i}\dot{\Psi}_i \tag{37}$$

Assumption A: The perturbation Ψ_i and its derivative $\dot{\Psi}_i$ are Lipschitz in their arguments and bounded over the domain of interest. In addtion, $\Psi(0) = 0$ and $\dot{\Psi}(0) = 0$.

Using $V_i(e, \eta) = V_{i0}(e_i) + W_i(\eta_i)$ as a Lyapunov function candidate for the closed-loop system (36) and (37), where

$$V_{i0}(e_i) = e_i^T P_{i1} e_i \tag{38}$$

over a ball $B(0, o_i) \subset R^3$, for some $o_i > 0$, and P_{i1} is the positive definite solution of the Lyapunov equation $P_{i1}A_{i0} + A_{i0}^T P_{i1} = -I_{i1}$, and

$$W_i(\eta_i) = \eta_{po_i}^T P_{i2}\eta_{po_i} \tag{39}$$

where P_{i2} is the positive definite solution of the Lyapunov equation $P_{i2}A_{po_i} + A_{po_i}^T P_{i2} = -I_{i2}$

Choose $\xi_i < o_i$; then, given Assumption A, we have, $\forall (e_i, \eta_{po_i}) \in B(0, \xi_i) \times \{\|\eta_{po_i}\| \le \xi_i\} = \Lambda_i$

$$\left|\dot{\Psi}_i(e_i, \eta_{po_i})\right| \le \gamma_{i2} \tag{40}$$

where γ_{i2} is an upper bound of $\dot{\Psi}$. $\forall (e_i, \eta_{po_i}) \in \Lambda_i$, then, we have

$$\begin{aligned} \dot{V}_i =& \frac{\partial V_{i0}}{\partial e_i}(A_{i0}e_i + B_i\eta_{i2}) \\ &+ \frac{\partial W_i}{\partial \eta_i}\left(\frac{1}{\epsilon_i}A_{po_i}\eta_{po_i} + B_{po_i}\dot{\Psi}_i\right) \\ =& -\|e_i\|^2 + 2e_i^T P_{i1}B_i\eta_{i2} - \frac{1}{\epsilon_i}\|\eta_{po_i}\|^2 \\ &+ 2\eta_{po_i}^T P_{i2}B_{po_i}\dot{\Psi} \\ \le& -\|e_i\|^2 - \frac{1}{\epsilon_i}\|\eta_{po_i}\|^2 + 2\|P_{i1}\|\|e_i\|\|\eta_{po_i}\| \\ &+ 2\gamma_{i2}\|P_{i2}\|\|\eta_{po_i}\| \\ \le& -\|e_i\|(\|x_i\| - 2\|P_{i1}\|\|\eta_{po_i}\|) \\ &- \|\eta_{po_i}\|\left(\frac{1}{\epsilon_i}\|\eta_{po_i}\| - 2\gamma_{i2}\|P_{i2}\|\right) \end{aligned} \tag{41}$$

Defining $\xi_{i2} = 2\epsilon_i\gamma_2\|P_{i2}\|$ and $\xi_{i1} = 2\epsilon_i\|P_{i1}\|\xi_{i2} = 4\epsilon_i\gamma_{i2}\|P_{i1}\|\|P_{i2}\|$; for any given $\xi_i \le o_i$, taking

$$\epsilon_i^* = \min\left\{\frac{\xi_i}{8\gamma_{i2}\|P_{i1}\|\|P_{i2}\|}, \frac{\xi_i}{4\gamma_{i2}\|P_{i2}\|}\right\} \tag{42}$$

Then $\forall \epsilon_i, 0 < \epsilon_i < \epsilon_i^*$, we have $\|e_i\| \le \frac{\xi_i}{2}, \|\eta_{po_i}\| \le \frac{\xi_i}{2}, \|e_i\| \ge \xi_{i1}$, and $\|\eta_{po_i}\| \ge \xi_{i2}$, which guarantees that

$$\dot{V}_i \le -\|e_i\|(\|e_i\| - \xi_{i1}) - \|\eta_{po_i}\|(\|\eta_{po_i}\| - \xi_{i2}) \le 0 \tag{43}$$

Thus, we have $T_i(\xi_i)$ and $T_1 > 0$,

$$\|e_i(t)\| + \|\eta_{po_i}\| \le \xi_{\mathrm{i}} \quad \forall t \ge T \tag{44}$$

Note 1: Verification of Assumption A. We have all physical variables of the closed-loop system are continuous and bounded. Therefore, both perturbation terms (Ψ_1, Ψ_2) and their derivatives are bounded based on equations (12) and (17). which ensures Assumption A satisfied.